Fluxgate three-component magnetometers for cost-effective ground, UAV and airborne magnetic surveys for industrial and academic geoscience applications and comparison with current industrial standards through case studies

Bruno Gavazzi, Pauline Le Maire, Jeanne Mercier de Lepinay, Paul Calou, Marc Munschy

Fluxgate three-component magnetometers for cost-effective ground, UAV and airborne magnetic surveys for industrial and academic geoscience applications and comparison with current industrial standards through case studies

Gavazzi B. (corresponding author)[1], Le Maire P.[1,2], Mercier de Lépinay J.[1], Calou P.[1,3], Munschy M.[1]

[1] Institut de Physique du Globe de Strasbourg, Ecole et Observatoire des Sciences de la Terre, Université de Strasbourg et CNRS (IPGS UMR71516), Strasbourg, France.
[2] CARDEM/EUROVIA, Bischeim, France.
[3] ECA-EN, Groupe ECA, Coueron, France.
bgavazzi@unistra.fr ; Phone +33368850473 ; mobile +33607639713 ; address: IPGS, 1 rue Blessig, 67084 Strasbourg Cedex, France

Abstract

In applied geophysics, magnetic methods are used in a wide range of industrial and academic applications with environmental, engineering or exploration components (e.g. military ordnance detection, pipe detection, archaeology, resources exploration, geological mapping). According to the type of application and the scale of the study, surveys can be conducted on the ground or airborne, each having its own industrial standard. In ground survey applications single component or scalar gradiometers are widely used. In airborne surveys the intensity of the magnetic field is measured with scalar magnetometers and the disturbances of the aircraft are compensated with real-time compensation unit.

This paper proposes another approach using the latest developments on the use of fluxgate three-component magnetometers. They have a light weight, a low power consumption, are rugged and allow a simple magnetic compensation of the carrier. They can provide a more precise and/or a more cost effective alternative to current measuring standards. They can also be mounted on UAVs to fill the gap in measurement capabilities between ground and airborne surveys, and therefore offer a new range of applications. A review of four case studies concerning archaeology, unexploded ordnance detection, lithology and structural geology studies is presented to illustrate the possibilities of application of such an approach and how it compares to current industrial standards in ground and airborne surveys.

1. Introduction

Applied Geophysics can be defined as the science of measurement and interpretation of physical properties to study sub-surface conditions. It plays therefore an important role in economic activities and academic research dealing with solid earth, from surface to the core, by providing non-intrusive and large scale data for imaging the underground. Practical applications are numerous[1], such as archaeology, engineering, environmental studies, mineral prospecting or hydrocarbon, geothermal and groundwater exploration. Different kind of methods exist, each based on a particular physical property. Geomagnetic methods consist in the measurement, processing and interpretation of spatial variations in the earth magnetic field linked to heterogeneities of the underground. They are passive methods, i.e. they are not based on reactions to external stimuli but on naturally occurring phenomena. They can be used in all the applications cited above, either in combination with other methods, or alone[1,2,3,4]. This vast range of potential applications led to the development of different methods and strategies for measuring the magnetic field depending on the scale and object of study: scalar or vector, gradient or total field, ground or airborne. However, the latest results on the use of vector magnetometers offer new possibilities for cost efficient and well compensated magnetic data acquisition on the ground, UAVs or aircrafts[5]. This paper aims to explore the industrial and scientific potentials of such possibilities through a discussion on the theory and current industrial standards, an explanation on how to use fluxgate three-component magnetometers for surveying and a review of case studies for different applications.

2. Main principles of geomagnetic methods and measuring standards

2.1 Main principles

Magnetism is a natural phenomenon resulting from movements of electrical charges at the atom level. These movements can be permanent (remanent magnetization) or a reaction to an external magnetic field (induced magnetization). At the macroscopic scale, materials can be characterized by their magnetization defined by a direction and an intensity in $A.m^{-1}$. Such magnetization is a sum of a remanent and an induced part. The remanent part is linked to the composition and formation processes of the material, while the induced part is also linked to the main geomagnetic field generated by deep internal sources (mainly the earth core). This main geomagnetic field varies in direction and intensity (from 20 000 to 70 000 nT on the surface) according to the position on the globe (mainly the latitude). Thus the magnetization of materials and associated magnetic fields are dependent on their composition as well as their geographical coordinates.

The basic principle of geomagnetic methods is to measure the magnetic field above the surface. This total magnetic field is a combination of the effect of all the sources, deep and superficial. Therefore,

heterogeneities of materials within the ground are generating spatial variations of the magnetic field above the surface, usually in the range of a few nT to a several 1000 nT in applied geophysical applications[6,7]. All geomagnetic methods consist in the quantification of such spatial variations, called anomalies, in the earth magnetic field. For each measurement, the magnetic anomaly can be defined as

$$\vec{A} = \vec{B} - \vec{R}\,, \tag{1}$$

where $\vec{A}$, $\vec{B}$ and $\vec{R}$ are the magnetic anomaly field, the measured total magnetic field and the main (or regional) geomagnetic field respectively. $\vec{R}$ is given by the International Geomagnetic Reference Field (IGRF) which is a model of the geomagnetic field based on data from surveys, magnetic observatories and satellites[8]. Due to technical limitations, only the intensity of the total magnetic field can be measured in motion accurately enough for applied geophysical applications. Therefore, the anomaly of the intensity, or total field anomaly, noted C, is defined as

$$C = \left\|\vec{B}\right\| - \left\|\vec{R}\right\|. \tag{2}$$

As $\left\|\vec{B}\right\| = \left\|\vec{A} + \vec{R}\right\|$ and $\left\|\vec{A}\right\| \ll \left\|\vec{R}\right\|$, equation (2) can also be written:

$$C \approx \left\|\vec{A}\right\| cos\,\alpha, \tag{3}$$

where α is the angle between $\vec{A}$ and $\vec{R}$. Thus the total field anomaly C is approximately equal to the component of $\vec{A}$ in the direction of $\vec{R}$. This means that if $\vec{R}$ can be considered as a constant, which is the case at scales used in applied geophysics, the total field anomaly C is a potential that satisfies Laplace's equation, i.e. it allows the use of potential field theory for interpretation.

2.2 Industrial measuring standards

Regardless of the measuring method, the main issues to obtain exploitable measurements are the reduction of the impact of natural and anthropogenic time-dependent variations (temporal correction) as well as the reduction of the impact of the magnetizations of the measuring device or carrier itself on the sensor (magnetic compensation). In addition, positioning should be managed carefully, as imprecision in positioning or too sudden variation of acceleration of the moving measuring device can lead to noise. Positioning systems offering 1 to 10 cm precision at 1 to 10 Hz are usually used. Natural time-dependent variations are linked to the sun activity and its interaction with earth. They consist of cycles of different periods (6 hours to tenths of years) with a daily variation that usually does not exceed 100 nT, as well as unpredictable magnetic storms with variations ranging up to a few hundred nT during a few hours to a few days. Anthropogenic variations are more local. They can be due to electromagnetic fields (e.g. generated by power lines) or metallic

masses in movement near the measurements (e.g vehicles). Their frequencies are usually higher than the hertz and with various intensities that can reach up to more than 10 000 nT. Variations due to the magnetizations of the device and carrier are dependent on the distance between magnetometers and the other components of the device as well as the composition, orientation and speed of the carrier. For example, a plane in a typical airborne survey can cause variations of 500-1000 nT with a standard deviation of more than 100 nT.

To address all these issues, different types of magnetometers or measuring strategies are used:

- For airborne surveys, the industrial standard is to use optically pumped alkali vapor (usually cesium) scalar magnetometers. They have a sensitivity of around 0.1 nT and can make measurements at a maximum frequency of 10 Hz. The temporal correction is evaluated from the data of a base station placed on the field or of a near magnetic observatory. The magnetic compensation is carried out with an automatic aeromagnetic digital compensation system (AADC) generating in real time a magnetic field opposed to the one of the aircraft according to its position and orientation[9,10]. The parameters of such a correction field are assessed and controlled for each survey through control flights in four directions (N, E, S, W) with pitch, roll and yaw movements. The residual error after correction during this maneuver should not excess 2 nT[10]. Parallel magnetic profiles are flown with a ratio height/spacing usually between 1:1 to 1:2.5. The height of the flight is fixed accordingly to the level of details required, usually between 50 and 500 m. Tie lines perpendicular to the profiles are also flown with a greater spacing. The differences at the crossing points between profiles and tie lines after all processing allow to assess the overall quality of the dataset, as it takes into account all sources of noise, such as positioning errors, uncompensated magnetizations or uncorrected time-dependent variations. The overall quality criterion depends on the study but is usually set under a few nT.

- For ground survey, industrial standards are less strict. The temporal correction is performed either with the use of a base station, as in aeromagnetic surveys, or by using a gradiometer for the survey: the difference in signal is recorded between two sensors placed at a fixed distance in any direction (often vertically). Thus the time-dependent variations can be considered the same on the two sensors and therefore do not influence the measurements. The compensation is usually not computed but the magnetometers are shifted from the rest of the equipment to reduce its impact. The most used devices are by far vector gradiometer (single-component fluxgates), but scalar gradiometers (alkali vapor or precession) and scalar magnetometers (alkali vapor or precession) are also used[3,11,12,13]. Sensors are usually positioned between 0.5 and 1 m above the ground. Parallel profiles are measured with a height/spacing ratio between 2:1 and 1:1 with both values between

0.25 and 1 m. Multi-sensor devices, especially vector gradiometers, are used to measure different profiles simultaneously and therefore increase surveying speed. They usually consist of 2 to 5 gradiometers that can be carried, pushed on a cart or pulled behind a vehicle. In contrast with airborne surveys, the overall quality of a dataset is usually difficult to assess as most of the time no quality control procedure, such as tie-line, is planned.

2.3 Signal processing and interpretation.

Different parameters have to be taken into consideration for interpretation of the magnetic data. The shape of the anomaly created by a magnetic source depends on the source 's magnetic and geometric properties, the distance between source and sensor as well as the properties of the regional magnetic field at the location which are mostly linked to its latitude . This can be illustrated through a synthetic case with buried structures of different magnetizations and shapes placed at different depths (Figure 1). The magnetic field of such structures can be computed from a distribution of simpler spherical sources of a radius a. The magnetic field $\vec{A}(x,y,z)$ of such source centered in $Q(x',y',z')$ at the observation point $P(x,y,z)$ is expressed as[6]

$$\vec{A}(x,y,z) = \frac{\mu_0}{4\pi}\frac{4\pi a^3}{3}\frac{j}{r^3}[3(\hat{j}.\hat{r})\hat{r} - \hat{j}], \quad \textbf{(4)}$$

where μ_0 is the magnetic permeability of empty space, j and $\hat{j}$ are the norm and the unit vector of the magnetization vector ($\vec{j} = j.\hat{j}$), and $\hat{r}$ and r are defined as $\overrightarrow{PQ} = \vec{r} = r.\hat{r}$. From equation (3) the magnetic anomaly $C(x,y,z)$ is approximated as the scalar product of $\vec{A}(x,y,z)$ with the unit vector of the regional field $\hat{R}$:

$$C(x,y,z) = \vec{A}(x,y,z) \cdot \hat{R}. \quad \textbf{(5)}$$

Equation (4) and (5) show two aspects of the magnetic anomaly illustrated on Figure 2, A and Figure 2, B: a magnetic anomaly always has a positive and a negative part and its intensity decreases with $1/r^3$. As a consequence, information on the geometry of the source are lost quickly with an increase in the distance to the source.

As $C(x,y,z)$ satisfies Laplace's equation, the spectral frequency w associated with z can be expressed as $w = i\sqrt{u^2+v^2}$, with u and v the frequencies associated with x and y. This means that it is possible to express the anomaly in the spectral domain through a 2D Fourier transform from a 2D survey and thus facilitate numerical computation as well as simplify several mathematical processes such as deconvolution or derivation[14]. Information on the position, geometry or magnetization of sources can be estimated through potential field transforms such as reduction to the pole, directional derivatives or analytic signel[6].

- Reduction to the pole (RTP, Figure 2, C-D) gives the anomaly a symmetrical shape centered on the source and can therefore be used to deduce its horizontal position[15]. It can be written

$$RTP = -\frac{u^2 + v^2}{\left(\alpha_R u + \beta_R v + \gamma_R i\sqrt{u^2 + v^2}\right)\left(\alpha_M u + \beta_M v + \gamma_M i\sqrt{u^2 + v^2}\right)} \quad \textbf{(6)}$$

where $(\alpha_R, \beta_R, \gamma_R)$ and $(\alpha_M, \beta_M, \gamma_M)$ are the directional cosines of the regional field and of the magnetization of the source respectively. The direction of the regional field and induced magnetization of the sources is given by IGRF but the direction of remanent magnetization of the sources is usually not known. The application of RTP to locate sources is therefore usually restricted to sources without remanent magnetization.

- Directional derivatives in direction $\vec{D}(\alpha, \beta, \gamma)$ can be written

$$\left[-i\left(\alpha u + \beta v + \gamma i\sqrt{u^2 + v^2}\right)\right]^n \quad \textbf{(7)}$$

where n is the order of derivative. Significant cases of directional derivatives are the vertical derivative (VD) and the horizontal derivative (HD) that can be expressed from equation (7) as

$$VD = \left(-\sqrt{u^2 + v^2}\right)^n \quad \textbf{(8)}$$

and

$$HD = \left(-i\sqrt{u^2 + v^2}\right)^n. \quad \textbf{(9)}$$

HD after RTP can be used to locate vertical contacts or vertical limits of a source [16]. VD (Figure 2, G-H) can be used to highlight short wavelengths and thus gain more information on the shape of shallow sources but also enhances noises.

- Vector analytic signal is a popular method to lo locate magnetized sources[2]. It is based on the fact that the vertical and horizontal derivatives of the anomaly can be defined as the real and imaginary part of a complex analytic signal[17]. Strictly speaking, only the norm of such an analytic signal is used. In 3D (SA, Figure 2, G-H) it is defined as[18]:

$$|SA| = \sqrt{\left(\frac{\partial C}{\partial x}\right)^2 + \left(\frac{\partial C}{\partial y}\right)^2 + \left(\frac{\partial C}{\partial z}\right)^2}. \quad \textbf{(10)}$$

For a perpendicular section of an elongated source, the maximum of SA gives the horizontal position of the source without a priori on its magnetization[17]. For other shapes, the maximum depends on both position and magnetic inclination and none can be accurately deduced[19]. However, if RTP can

be applied, the position, depth and magnetic moment of spherical sources can be estimated through an inverse problem[20].

As demonstrated, these interpretative methods can be applied on the defined anomaly as it is a potential that satisfies Laplace's equation. In comparison, data obtained with gradiometers are a difference of measurement between two sensors of which the absolute position is not well known. Therefore, the assumption about the difference being a gradient might be inaccurate, especially for ground surveys over shallow sources. In this case the application of interpretative methods cited before might be hazardous and is not recommended. In conclusion, the adapted solution will be different according to the application and budget of the survey.

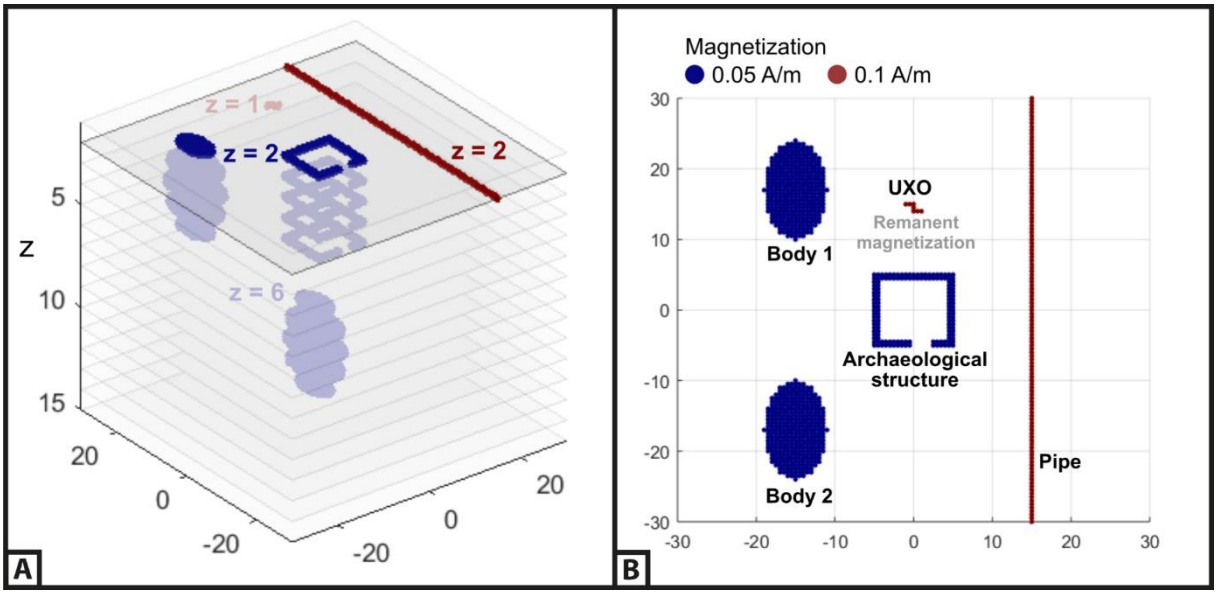

Figure 1: Synthetic case of buried structures of different shape and magnetization. X and Y axis toward East and North respectively. Z axis corresponds to depth. A - 3D block model. B - Planar overview. Magnetic inclination and declination are set to 40 and 15 degrees respectively for all sources (induced magnetization) except for the UXO for which inclination and declination are set to 60 and -18 degrees to simulate remanent magnetization.

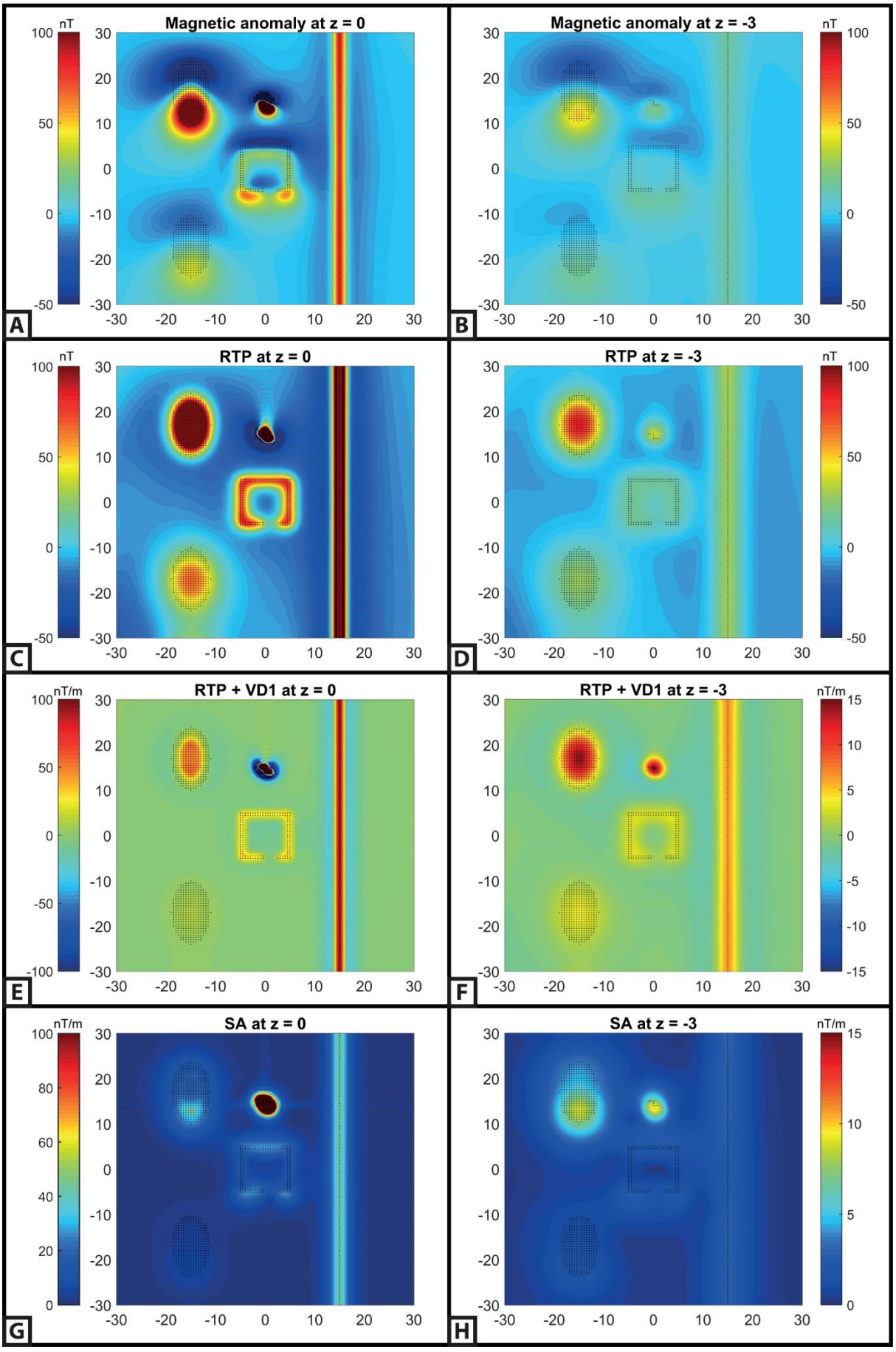
Magnetic anomaly at z = 0
Magnetic anomaly at z = -3
RTP at z = 0
RTP at z = -3
RTP + VD1 at z = 0
RTP + VD1 at z = -3
SA at z = 0
SA at z = -3
nT
nT/m
A
B
C
D
E
F
G
H

191

Figure 2: Map of the magnetic anomalies and potential field transforms of the synthetic case presented in Figure 1. Left column corresponds to a level on the surface (z=0) and the right column to a level at 3 m of altitude (z = -3). A/B - Magnetic anomaly. C/D - Reduction do the pole (RTP). E/F - First order vertical derivative (VD1). G/H - Vector analytic signal (SA).

3. How to use Fluxgate three-component magnetometers in applied geophysics

Fluxgate three-component magnetometers are electronic sensors measuring the intensity of the magnetic field in three orthogonal directions. They are therefore vector magnetometers[21]. They are light, robust and have a low power consumption. Despite these advantages, they are relative instruments with inherent errors of offset, sensitivity and angle (non-orthogonality). That is why they were abandoned for surveying in the 1960's, except for heading correction in AADC systems. However, Munschy et al[20] showed that such magnetometers can be calibrated and the equipment mathematically compensated from a simple procedure at the beginning of each survey. This procedure consists in recording the three components of the magnetic field while moving the whole system (sensors, digitizer and carrier) in every direction in an area where the magnetic field is known. On the ground it consists in an area of 1-2 square meters where the device is rotated by 360° around a fixed point (yaw) while roll movements of +/- 45° are applied. With an airborne carrier the maneuver consists in flying a clover shape route at a fixed altitude while performing roll movements. The differences between each three component measurement $F = \left(F_x, F_y, F_z\right)^T$ and the known magnetic field $B = \left(B_x, B_y, B_z\right)^T$ can thus be associated with noises due to the sensor itself as well as the magnetizations of the equipment according to the following equation[20]:

$$F = E_O + E_S * E_A * B, \tag{11}$$

where E_O, E_S and E_A correspond to the errors of offset O, sensitivity s and non-orthogonality γ for each component of the magnetometer such as

$$E_0 = \begin{pmatrix} O_x \\ O_y \\ O_z \end{pmatrix}, \tag{12}$$

$$E_S = \begin{pmatrix} s_x & 0 & 0 \\ 0 & s_y & 0 \\ 0 & 0 & s_z \end{pmatrix}, \tag{13}$$

$$E_A = \begin{pmatrix} 1 & 0 & 0 \\ -sin\,\gamma_x & cos\,\gamma_x & 0 \\ sin\,\gamma_y & sin\,\gamma_z & \sqrt{1 - sin^2\,\gamma_y - sin^2\,\gamma_z} \end{pmatrix}. \tag{14}$$

If enough measurements in enough directions are made, i.e. enough different F are measured, the 9 parameters O_x, O_y, O_z, s_x, s_y, s_z, γ_x, γ_y, γ_z of the equations (12), (13) and (14) can be estimated through a linearized least-square inverse problem consisting in minimizing by iteration the misfit between measured value and known magnetic field. Once the parameters are estimated, a corrected value F_C of the magnetic field for each measurement F can be calculated as follows:

$$F_C = {E_A}^{-1} * {E_S}^{-1} * (F - E_O). \quad \textbf{(15)}$$

Thereby, the intensity of the magnetic field can be computed with a precision suitable for applied geophysics and with higher sampling rates than scalar magnetometer. For example, Institut de Physique du Globe de Strasbourg (IPGS) uses Bartington MAG03 fluxgate three-component magnetometers to survey at sampling frequencies from 25 to 300 Hz, while scalar magnetometers usually have a maximal sampling rate of 10 Hz. For the Bartington MAG03 used by IPGS, the manufacturer gives errors of offset, sensitivity and angle of +/- 5 nT, less than 0.0015 % and less than 0.5° respectively, which are typical values for high-end fluxgate magnetometers. This is translated by variations during a calibration and compensation procedure with a standard deviation (STD) of approximately 20 nT. After correction, the STD drops to less than 2 nT[20]. The STD of the corrected values does not depend on the magnetization of the equipment which only affects the STD before correction[22]. However, this result depends on how well the geomagnetic field is known over the area where the compensation procedure is carried out . Usually after correction of the time-dependent variations it can be considered a constant value given either by the IGRF or the median value of the data, but variations of a few nT between the assessed and real values can occur. When the magnetic field is well known, i.e. there is no differences between assessed and real values, STD after correction below 0.5 nT can be obtained[23]. IPGS developed a measuring system which can be mounted on any carrier on the ground or airborne[5]. Its light weight and compensation ability make it especially adapted to be carried by light unmanned aerial vehicles. This opens the range of applications by covering the gap of scale of measurements between ground and airborne surveys. IPGS integrated its system with Bartington MAG03 on different carriers, of which the most commonly used are:

- Ground surveys: IPGS uses a multi-sensor device mounted on a backpack using up to eight fluxgate three-component magnetometers placed 0.8 m above the ground to measure simultaneously parallel magnetic profiles with a line spacing of 0.5 m (Figure 3). The compensation ability allows the device to be compact and to integrate additional equipment such as D-GNSS antenna or real time display of magnetic and navigation data[20,23].

- UAV surveys: IPGS uses a mono-sensor device using one fluxgate three-component magnetometer mounted on a light UAV, such as a DJI matrice 100. The magnetometer is slightly shifted from the

246 engines, as they are generating time-dependent variations that as such cannot be compensated. The
247 calibration and magnetic compensation of the rest of the equipment (UAV, GNSS antenna) is
248 completed through a maneuver where the UAV performs roll and yaw over an area of a few square
249 meters at a fixed elevation (usually 50 m), in a way similar to the procedure for ground devices. The
250 UAV can acquire data at speed ranging from 3 to 60 km/h, at elevation between 1 and 200 m above
251 the ground, either draping the topography or at a fixed level. Distance to ground is either planned
252 beforehand from a numerical model or assessed in real time with a laser depending on the
253 availability and resolution of an elevation model of the area as well as the risk of unplanned obstacles
254 such as vehicles or vegetation for surveys carried at very low elevation (usually less than 30 m).

255 - Airborne surveys: IPGS uses a mono-sensor device mounted on a simple aircraft[22], a gyrocopter[24] or
256 ultra-light aircraft[5]. The calibration and compensation procedure is carried out through a clover
257 shaped figure.

258 Figure 3 shows uncorrected and corrected measurements obtained through the typical calibration
259 and compensation procedure explained above as well as the average STD before and after correction
260 for a single magnetometer and different carriers (ground, UAV, airborne). The differences of STD
261 after corrections between carriers are mainly explained by unknown variations of the magnetic field
262 in the area of the procedure but could also indicate uncorrected time-dependent variations (such as
263 electromagnetic fields from the battery or engine) or a difference of the number of visited attitudes
264 during the procedure which are usually lower with airborne carrier than on the ground. Regardless of
265 the carrier, the STD after correction is always lower than 2 nT.

266

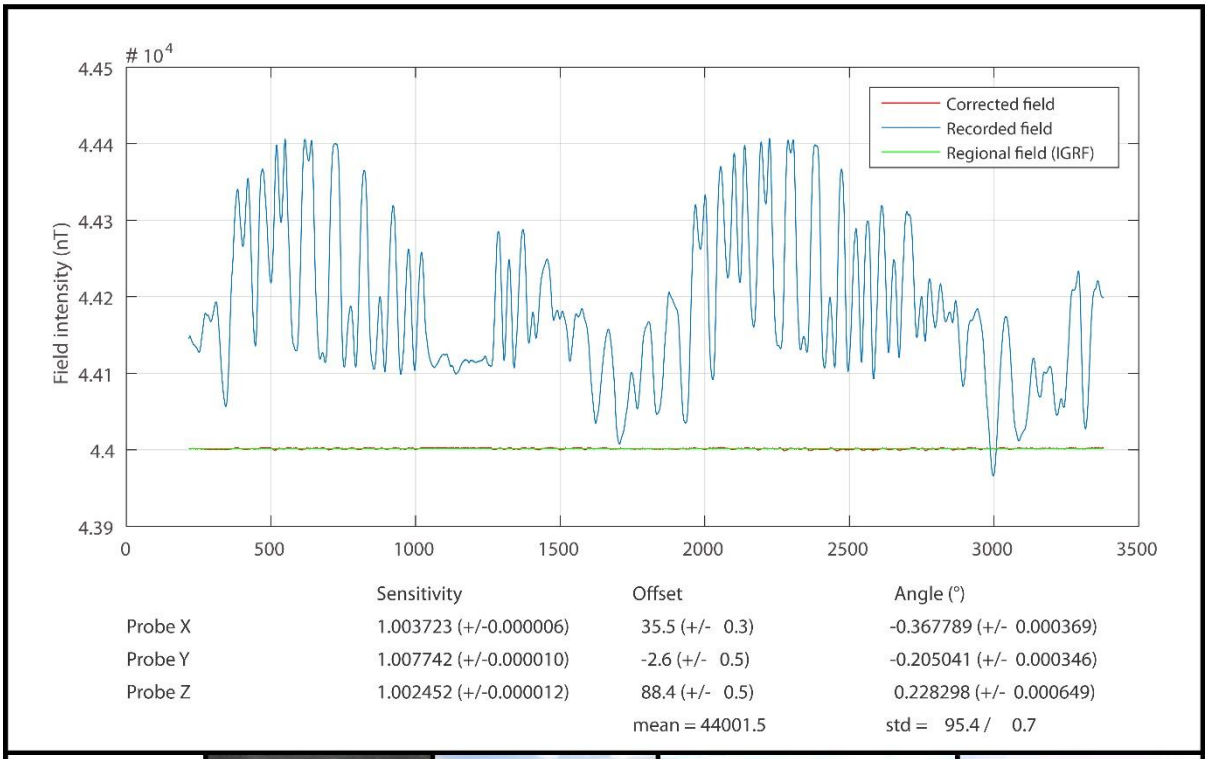

Measuring system	Magnetometer	Backpack system	UAV (DJI Matrice 100)	Aircraft (Maule MX7)
STD before procedure	21	97	54	102
STD after procedure	0.3	0.7	1	1.9

Figure 3: Intensity of the magnetic field measured by one fluxgate three_component magnetometer (Bartington MAG03) during the calibration and compensation process of the backpack mounted device. The raw data is shown in blue, corrected data in red and regional field in green. Applied correction parameters (sensitivity, offset and angle) for each probe of the sensor are shown below the curves. The table shows the standard deviation before and after the corrections of the calibration and compensation procedure for different carriers.

4. Case study

In order to assess the possibilities offered by the use of fluxgate three-component magnetometers, a few examples of application at different scales and with different carriers are presented. Case studies 1 and 4 are partially published in Gavazzi et al.23 and Munschy and Fleury22 respectively while 2 and 3 are unpublished work form IPGS.

4.1 On the ground: high resolution for archaeological applications

During the study of the site of Qasr 'Allam in the oasis of Bahariya in the Western desert of Egypt, an area was surveyed by two measuring system, as reported by Gavazzi et al.[23]: the backpack mounted system (Figure 3) in the framework of a collaboration between archaeologists and IPGS, and a

283 vertical component gradiometer very common in archaeological and other near-surface applications
284 (Geoscan FM 256) in the framework of a commercial service conducted by a team of the Institute of
285 Archaeology and Ethnology of the Polish Academy of Sciences. The two devices measure different
286 physical quantities: the vertical component gradient for the gradiometer and the total magnetic field
287 intensity for the backpack system. However, gradient and intensity can be calculated from one
288 another using potential field theory: gradient is a derivative of intensity and therefore intensity an
289 integral of gradient, both easily calculated in the spectral domain after a gridding step. Thus
290 calculated and measured quantities for each dataset can be compared and should be similar.
291 Gridding is done with a 0.25 m step and the measured and calculated anomaly of the total magnetic
292 field and vertical component gradient are shown in Figure 4. The two maps of vertical gradient are
293 mostly similar as expected, the slight differences being due to different level of imprecision for the
294 two surveys as well as slight differences in distance to the ground of the sensors. The two maps of
295 the anomalies of the total magnetic field show strong differences: large wavelength anomalies
296 appear on the map calculated from the measured gradient compared to the measured anomalies.
297 This cannot be due to edge effects which should be following the direction of the axes x and/or y.
298 The differences are mainly due to imprecisions in the measurements that are enhanced through the
299 calculation process. Indeed, the fact that the two sensors of a gradiometer cannot be maintained
300 exactly vertical during the survey leads to imprecisions small enough to be considered not significant
301 when the gradient is directly displayed but important enough to pose problem in potential field
302 calculations. Thus Figure 4 illustrates why using interpretative methods from potential field theory on
303 gradiometers data can be hazardous and is not recommended. In the case of the study, most of the
304 anomalies have short wavelengths and can be interpreted on both surveys as irrigation channels
305 while anomalies with large wavelengths, corresponding to deeper sources such as older channels and
306 wells can only be interpreted on the results of the backpack system. Another difference between the
307 two systems is the surveying time for the same area: approximately two days for the survey with a
308 single gradiometer and one hour for the survey with the backpack system. The greater speed of the
309 backpack system is due to its multi-sensors aspect as well as the integration of real time positioning
310 using a GNSS system. Thus the system allows to acquire four simultaneous profiles with no
311 preparations on the field while the gradiometer allows to measure only one profile at a time and
312 requires the set-up of a georeferenced grid on the field. Such step can take more time than the
313 recording itself.

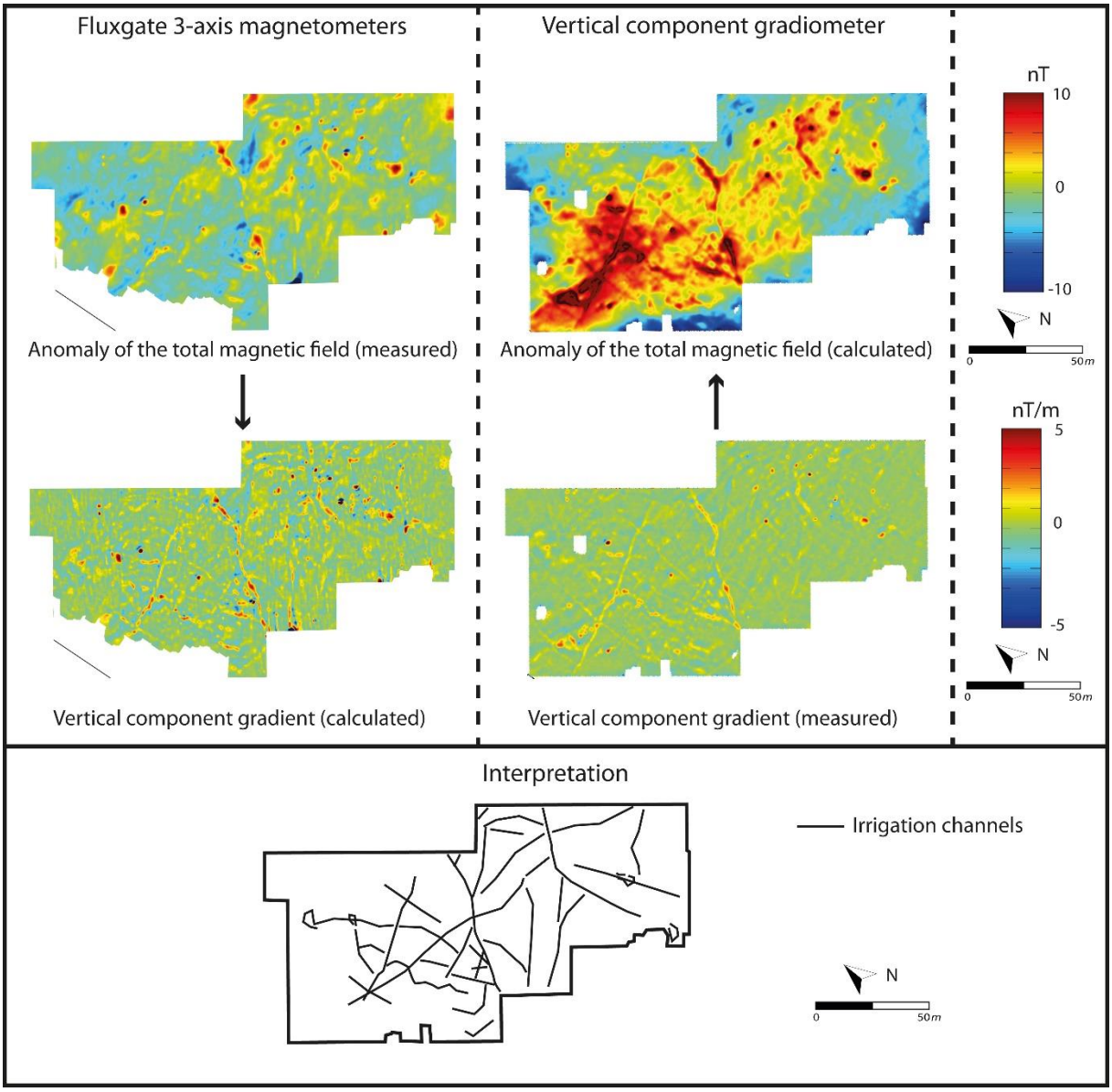

Figure 4: Comparison of two surveys of the same area with different devices and resulting interpretation. Anomaly of the total magnetic field and vertical component gradient are either measured or computed according to the surveying device.

4.2 UAV-borne and ground surveys for the detection of Unexploded Ordnance

The former French army aerial base BA112 contains many residues of the two last world wars: unexploded ordnance (UXO), ammunition stocks, trenches, tunnels... In the framework of a collaboration between CARDEM and IPGS an area was surveyed with different devices using fluxgate three-component magnetometers to assess the anthropogenic pollution of the underground as well as to compare the limit of detection of different carriers. A ground survey at 0.8 m above the ground was conducted with a backpack system as well as an UAV survey 3 m above ground level with a greater speed but lower resolution than the ground survey. Figure 5-A presents the observed maps of the magnetic anomaly for the two surveys and the corresponding maps of the vector analytic

signal to assess the horizontal position of the sources. As the distance of sensors to the ground increases, the wavelengths of the anomalies increase and their amplitudes decrease. The orange, blue and green lines on the interpretative map in Figure 5-B show different patterns of anomalies. The orange lines highlight the presence of buried networks or pipes, the green line highlights a part of a trench from the first world war and the blue lines highlight the remains of an old building. All dipole anomalies might correspond to UXO as well as other concentrated metallic material. Depth and magnetization of these potential UXO are evaluated from each dataset through an inverse problem on the analytic signal, assuming a spherical geometry (i.e. that the UXO are compact) and after a reduction to the pole assuming only induced magnetization. This assumption is common in UXO detection due to a great reduction of the remanent magnetization by the shock of firing and impact[25]. Three anomalies are selected to illustrate the limits of the method:

- Source A: the digging revealed a piece of wire mesh at a depth of 0.54 m, similar to the estimated depth from the two dataset (0.5 and 0.7 m, the difference is explained by the lower accuracy level of the GNSS antenna mounted on the UAV than on the backpack). The estimated magnetization from the UAV survey (44.5 $A.m^2$) is twice the one from the backpack survey (18.2 $A.m^2$).

- Source B: the digging revealed three screw pickets at a depth of 0.68 m, similar to the depth given from the backpack survey (0.7 m). The UAV survey gives an overestimated depth (1.1 m), probably due to the lower accuracy of the GNSS antenna. The estimated magnetization from the backpack survey (74.2 $A.m^2$) is twice the one from the UAV survey (42 $A.m^2$).

- Source C: the digging revealed 14 screw pickets, barbed wire and shrapnel at a depth of 1.28 m, which differs greatly from the depth given from the backpack survey (2.5 m) and UAV survey (0 m). The estimated magnetization from the backpack survey (4738 $A.m^2$) is five times the one from the UAV survey (884 $A.m^2$).

The differences in depth and magnetization estimations can be due to the non-spherical geometry of the sources. Indeed, depth estimations for sources A and B which consist in 1 and 3 objects are consistent with field evidences while the estimations for source C which consists in 14 objects are not consistent and differ with the field evidence. A similar effect seems to impact the estimation of magnetization but with a greater extent, as none of the estimated values are consistent. A presence of remanent magnetization could also play a role in these inaccuracies. In conclusion, both surveys seem to provide a good lateral position of the different sources but depth and magnetization estimations should be used cautiously as they can lead to significant errors if the sources are not a compact enough or composed of several objects.

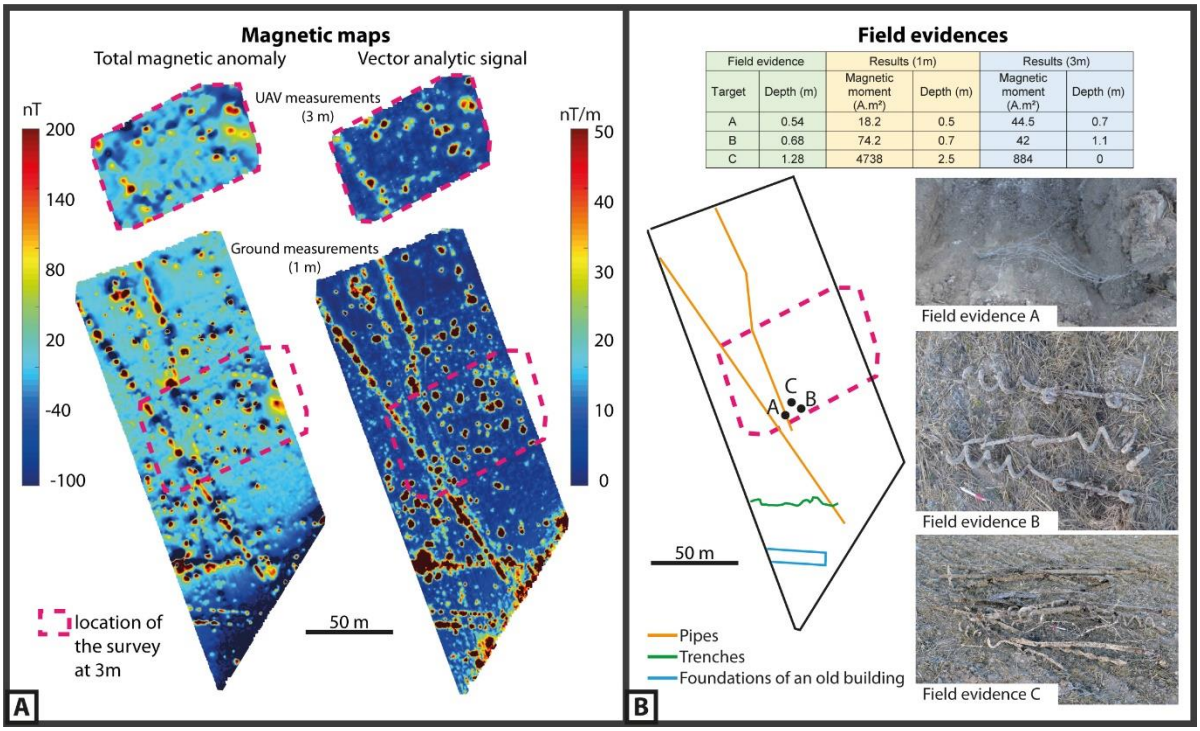

Figure 5: A - Maps of the magnetic anomalies to the left and maps of the vector analytic signal to the right for the two surveys (UAV and Backpack). B - Interpretative map of significant structures (trenches, pipes and old building) and comparison of interpretation and field evidence obtained for dipole anomalies A, B and C.

4.3 UAV-borne surveys for high resolution lithological and structural studies

A magnetic cartography using a light UAV was performed by IPGS in collaboration with Teranov in the framework of St kitts geothermal project. The goal of the survey is to improve the geological structural interpretation of a part of the island. Because of the dense vegetation and steep topography (slope angles reach more than 35°), ground measurements are almost impossible. Airborne magnetic measurements are also ruled out for the same reason: an airplane cannot follow such a topography at a low altitude.

A light UAV (DJI Matrice 100) equipped by IPGS with a Bartigton fluxgate three-component magnetometer was used to produce a draping magnetic map 100 m above ground, with a line-spacing of 100 m and for a total area of 13 km². From June 27th to July 1st 2016, the UAV has flown 218 km distributed in 107 km of profiles, 30 km of tie-lines and 81 km for transit (Figure 6, A). The resulting dataset was used to compute the total magnetic intensity. The anomaly of the magnetic intensity map presented in figure 6, A is computed by removing the regional field given by the IGRF from the data after correction of the time-dependent variations. This first map shows SW-NE directions consistent with the local fault network[26,27] and a circular anomaly correlated to the Brimstone hill andesitic dome[28,29].

One major direction near Brimstone hill was identified as an area of interest. To better understand the magnetic anomalies in this specific zone, a 25 m above ground draping survey was conducted. This survey was flown with a 25 m line-spacing between the 2nd and the 5th of July 2016 for a total of 28 km of magnetic profiles and tie-lines and an area of 0.65 km². The resulting anomaly map is overlaid on the previous 100 m survey on Figure 6, B.

The contribution of the 25 m survey is better seen on Figures 6, C and 6, D presenting the reduction to the pole of the magnetic anomaly in the area of interest. The large SW-NE direction previously identified is revealed to be constituted of two smaller and discontinued lineaments as shown in figure 6, E and 6, F. The discontinuity of these anomalies indicates the presence of a structural direction N020 that was not previously recognized in this area.

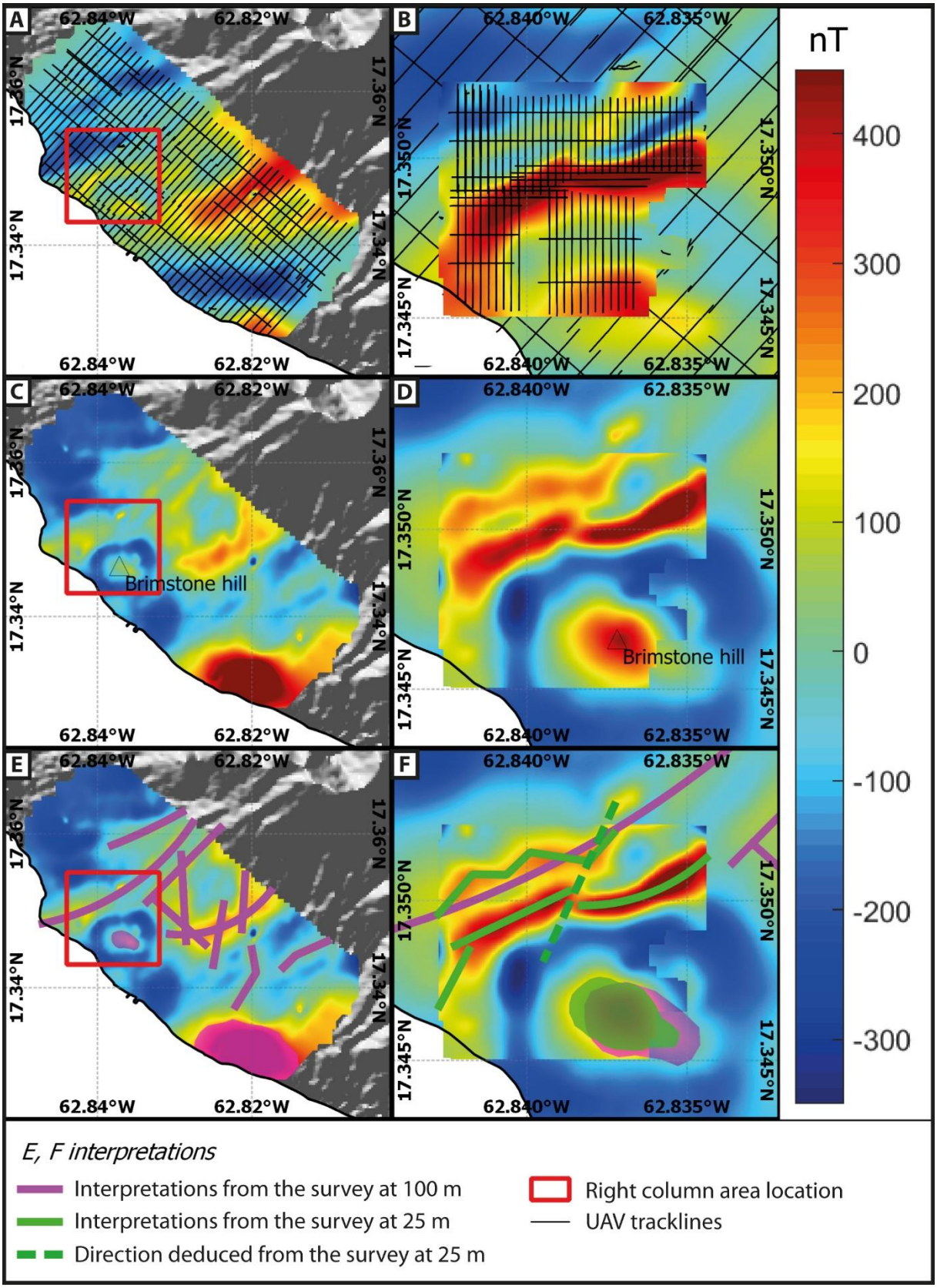

Figure 6: Saint Kitts UAV surveys. Left column: 100 m above the ground survey, Right column: superposition of 100 m and 25 m above the ground surveys, zoomed in the red squares. A/B - Maps of the anomalies of the total magnetic intensity. C/D/E/F - Maps of the reduction to the pole of the anomalies. Color scales are kept consistent for all surveys and representations.

4.4 Airborne surveys for large scale lithological and structural studies and comparison with industrial standard

In the framework of a geothermal exploration project, two surveys were conducted in the Vosges mountain with different measuring systems. A first survey at a fixed level of 1000 m above sea level was conducted in 2008 by IPGS with its own measuring system using one Bartington fluxgate three-component magnetometer mounted on a Maule MX7. The second survey took place in 2015 and was executed by the geophysics contractor *eGeophysics GPR international Inc.* with an absolute Geometrics cesium magnetometer mounted on a custom helicopter Ecureuil AS350 and a RMS Instruments AADC for real time compensation. This survey draped the topography at 300 m above ground level and the altitude of the data is varying between 400 and 1400 m above sea level. Both surveys are overlapping in an area of roughly 20 x 10 km but at different altitudes. In order to compare both datasets an upward continuation to the level of the highest data point (1400 m) is calculated. The resulting maps are shown in Figure 7. The different anomalies correspond to structural features or lithological contacts that will be discussed with geologists. In the overlapping area, no differences are visible between the results of the two different devices, thus illustrating a similar level of quality of data between a system using a fluxgate three-component magnetometer and an industrial system using a cesium magnetometer. The main difference lies in the cost: the system used by IPGS costs around 5 k€ while scalar magnetometers have a higher price range (15 k - 50 k€) and require the addition of an AADC (100k - 200 k€) for the magnetic compensation of the carrier. Thus, for a same carrier, the difference of price between the two types of measuring systems is of a factor ranging between 20 and 50.

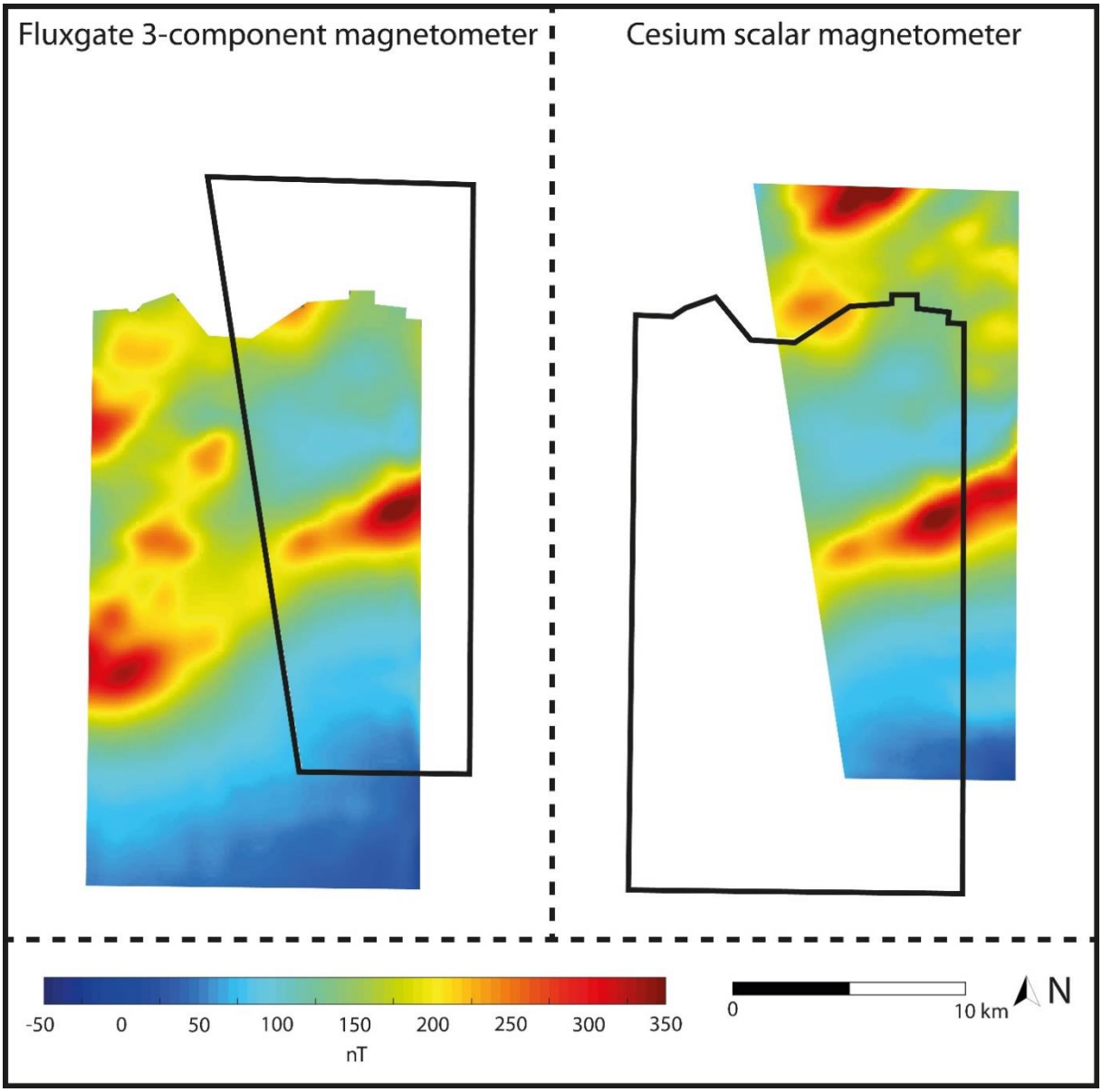

Figure 7: Comparison of results of magnetic surveys over the same area in the Vosges mountains with two different systems: Left - survey conducted in 2008 by IPGS with a Maule MX7 with Bartington MAG03 fluxgate three-component magnetometers; right - survey conducted in 2015 by Geophysics GPR International Inc. with a AS 350 Ecureuil with Geometrics Cesium scalar magnetometer and a RMS instruments compensation system.

5. Conclusion

As illustrated by the different examples, measuring systems using fluxgate three-component magnetometers can be a good alternatives to different standards in use in applied geophysics. In airborne surveys, they provide results with the same quality and precision than industrial systems based on scalar magnetometers at a fraction of their cost (20 to 50 times less). In ground surveys, they are often faster than other devices and the results are less prone to noise than gradiometer results when interpretative potential field transformations are used. In addition, they can be

mounted on light UAVs and aircrafts, filling the scale gap between detailed ground surveys and regional airborne surveys. This ability to survey at any scales offers new resolution of data and thus new possibilities of application. The system developed by IPGS is currently used for archaeology, UXO detection, pipe detection and resources exploration but could be used in any application where heterogeneities within the ground must be assessed.

5. Acknowledgement

The authors would like to thank different partners for their support and providing some of the dataset: Teranov for the UAV survey of St Kitts and their continuous support; Fonroche Energie for providing data of the helicopter-borne survey in the Vosges. CARDEM and CEA for supporting the surveys on the BA112 and Tomasz Herbich and his team for the gradiometry survey. The authors would also like to thank the Initiatives d'Excellence (Idex, Programme Investissements d'Avenir) of the Université de Strasbourg for their financial support for the survey on the archaeological site of Qasr 'Allam. We thank Dimitrios Terzis and two anonymous reviewers for their comments and suggestions that greatly improved the manuscript.

Bibliography

1. Reynolds JM. *An introduction to applied and environmental geophysics*. John Wiley & Sons; 1997.

2. Nabighian MN, Grauch VJS, Hansen RO, et al. The historical development of the magnetic method in exploration. *Geophysics*. 2005; 70(6): 33ND–61ND. doi: 10.1190/1.2133784

3. Linford N. 2006. The application of geophysical methods to archaeological prospection. *Rep on Prog in Phys*. 2006. 69: 2205-2257. doi: 10.1088/0034-4885/69/7/R04

4. Liu Q, Roberts AP, Larrasoaña JC, et al. Environmental Magnetism: principles and applications. *Rev of Geophys*. 2012; 50(4): RG4002. doi: 10.1029/2012RG000393

5. Gavazzi B, Le Maire P, Munschy M, Dechamp A. Fluxgate vector magnetometers: A multisensor device for ground, UAV, and airborne magnetic surveys. *The Lead Edge.* 2016; 35(9): 795-797. doi: 10.1190/tle35090795.1

6. Blakely RJ. *Potential Theory in Gravity & Magnetic Applications*. Cambridge University Press; 1995.

7. Telford W, Geldart L, Sheriff R. *Applied Geophysics*. Cambridge University Press; 1990. doi: 10.1017/CBO9781139167932

8. Thébault E, Finlay CC, Begga CD, Alken P, Aubert J, Barrois O, Bertrand F, Bondar T, Boness A, Brocco L, Canet E, Chambodut A, Chulliat A, Coïsson P, Civet F, Du A, Fournier A, Fratter I, Gillet N, Hamilton B, Hamoudi M, Hulot G, Jager T, Korte M, Kuang W, Lalanne X, Langlais B, Léger JM, Lesur V,

461 Lowes FJ, Macmillan S, Mandea M, Manok C, Maus S, Olsen N, Petrov V, Ridley V, Rother M, Sabaka
462 TJ, Saturnino D, Schachtschneider R, Sirol O, Tangborn A, Thomson A, Tøffner-Clausen L, Vigneron P,
463 Wardinski I, Zvereva T. International Geomagnetic Reference Field: the 12th generation. *Earth,*
464 *Planets and Space.* 2015. 67:79. doi: 10.1186/s40623-015-0228-9

465 9. Horsfall KR. Airborne magnetic and gamma-ray data acquisition. *AGSO J of Aust Geol & Geophys.*
466 1997; 17(2): 23-30

467 10. Coyle M, Dumont R, Keating P, Kiss F, Miles W. Geological Survey of Canada aeromagnetic
468 surveys: design, quality assurance, and data dissemination. *Geological survey of Canada*, open file
469 7660. doi: 10.4095/295088

470 11. Butler DK. Implications of magnetic backgrounds for unexploded ordnance detection. *J of Appl*
471 *Geophys*. 2003; 54 (1-2): 111-125. doi: 10.1016/j.jappgeo.2003.08.022

472 12. Gaffney C. Detecting trends in the prediction of the buried past: A review of geophysical
473 techniques in archaeology. *Archaeom*. 2008; 50: 313–336. doi: 10.1111/j.1475-4754.2008.00388.x

474 13. Zalevsky Z, Bregman Y, Salomonski N, Zafrir H. Resolution Enhanced Magnetic Sensing System for
475 Wide Coverage Real Time UXU Detection. *J of Appl Geophys.* 2012; 84: 70-76. doi:
476 10.1016/j.jappgeo.2012.06.003

477 14. Bhattacharyya BK, Navolio ME. A fast fourier transform method for rapid computation of gravity
478 and magnetic anomalies due to arbitrary bodies. *Geophysic Prospect.* 1976; 24: 633-649. doi:
479 10.1111/j.1365-2478.1976.tb01562.x

480 15. Baranov V. 1957. A new method for interpretation of aeromagnetic maps: pseudo gravimetric
481 anomalies. *Geophys*. 1957; 22: 359-383. doi: 10.1190/1.1438369

482 16. Grauch VJS, Cordell L. Limitations of determining density or magnetic boundaries from the
483 horizontal gradient of gravity or pseudogravity data. *Geophys*. 1987; 52(1): 118–121. doi:
484 10.1190/1.1442236

485 17. Nabighian MN. The Analytic Signal of Two-Dimensional Magnetic Bodies with Polygonal Cross-
486 Section; Its Properties and Use for Automated Anomaly Interpretation. *Geophys.* 1972; 37(3):
487 507-517. doi: 10.1190/1.1440276

488 18. Roest WR, Verhoef J, Pilkington M. Magnetic Interpretation Using the 3-D Analytic Signal.
489 *Geophys.* 1992*;* 57(1): 116-25. Doi: 10.1190/1.1443174

490 19. Salem A, Ravat D, Gamey TJ, Ushijima K. Analytic signal approach and its applicability in
491 environmental magnetic investigations. *J of Appl Geophys*. 2002; 49(4): 231–244. doi:
492 10.1016/S0926-9851(02)00125-8

493 20. Munschy M, Boulanger D, Ulrich P, Bouiflane M. Magnetic mapping for the detection and
494 characterization of UXO: Use of multi-sensor fluxgate 3-axis magnetometers and methods of
495 interpretation. *J of Appl Geophys*. 2007; 61: 168-183. doi: 10.1016/j.jappgeo.2006.06.004

496 21. Primdahl F. The fluxgate magnetometer. *J of Phys E: Sci Instrum*. 1979; 12(4): 241-253. doi:
497 10.1088/0022-3735/12/4/001

498 22. Munschy M, Fleury S. Scalar, vector, tensor magnetic anomalies: measurement or computation?
499 *Geophys Prospect*. 2011; 59: 1035-1045. doi: 10.1111/j.1365-2478.2011.01007.x

500 23. Gavazzi B, Alkhatib-Alkontar R, Munschy M, Colin F, Duvette C. On the Use of Fluxgate 3-Axis
501 Magnetometers in Archaeology: Application with a Multi-sensor Device on the Site of Qasr 'Allam in
502 the Western Desert of Egypt. *Archaeol Prospect*. 2017; 24(1): 59-73. doi: 10.1002/arp.1553

503 24. Ameglio L, Jacobs G, Von Ludwig J, Munschy M. GyroLAG - fluxgate magnetic total field, vectors,
504 and tensors mapping. *The Lead Edge.* 2011; 30(6): 674-680. doi: 10.1190/1.3599154

505 25. Billings S, Beran L. Experimental measurements of shock induced changes to the magnetization of
506 unexploded ordnance. *J of Appl Geophys.* 2014; 105: 138-146. doi: 10.1016/j.jappgeo.2014.03.015

507 26. Feuillet N, Leclerc F, Tapponnier P, et al. Active faulting induced by slip partitioning in Montserrat
508 and link with volcanic activity: New insights from the 2009 GWADASEIS marine cruise data. *Geophys*
509 *Res Lett*. 2010; 37(19): L00E15. doi: 10.1029/2010GL042556

510 27. Feuillet N, Beauducel F, Tapponnier P. Tectonic context of moderate to large historical
511 earthquakes in the Lesser Antilles and mechanical coupling with volcanoes. *J of Geophys Res: Solid*
512 *Earth*. 2011; 116: B10308. doi: 10.1029/2011JB008443

513 28. Baker PE. The geological history of Mt Misery Volcano, St Kitts, West Indies. *Overseas Geol and*
514 *Miner Resour*. 1969; 10(3): 207-230. doi: 10.1016/S0024-4937(68)80004-0

515 29. Roobol MJ, Smith AL. *Geological map of St. Kitts, West Indies;* 2015